ELSEVIER

Optical Materials 14 (2000) 81–90

OPTICAL Materials

www.elsevier.nl/locate/optmat

Diode pumping Nd-laser efficiency limitations due to up-conversion processes in Nd:YLF and Nd:GLF

Lilia Coronato Courrol *, Edison Puig Maldonado, Laércio Gomes, Nilson Dias Vieira Jr., Izilda Marcia Ranieri, Spero Penha Morato

Instituto de Pesquisas Energéticas e Nucleares – Divisão de Materias Optoeletrônicos, Caixa Postal 11042, Pinheiros, 05422-970 São Paulo, Brazil

Received 28 October 1998; accepted 27 September 1999

Abstract

The visible up-conversion fluorescences mainly from the $^4G_{7/2}$ level in Nd-doped $LiYF_4$ and $GdLiF_4$ crystals have been studied at 300 K under c.w. diode laser pumping at 797 nm. These emissions originate from either two-step excitations, involving an excited-state absorption (ESA) from the $^4F_{3/2}$ metastable level or from energy transfer up-conversion (ETU) processes. A model to estimate the probability rates of the ETU processes based on the Förster–Dexter method was proposed. By solving the rate equations for these systems under continuous diode pumping, it was possible to calculate the pumping efficiencies in order to attain the threshold conditions for the 1.047 μm laser action, which showed a non-linear behavior. The theoretical calculations clearly indicate that the maximum possible inverted population (at the $^4F_{3/2}$ level) is around one-tenth of the total Nd concentration, for both crystals. The maximum gain is thus limited by the decrease of pumping efficiencies due to the up-conversion processes at the laser threshold.

PACS: 42.55.f; 33.50-j

Keywords: Diode-pumped lasers; Energy transfer

1. Introduction

With the development of powerful diode lasers emitting around 800 nm, spectroscopic studies of insulating laser crystals doped with Nd^{3+} were renewed. All solid-state Nd laser systems pumped by high-power diode lasers have high efficiencies and are now standard tools for many applications [1,2]. In particular the Nd-doped $YLiF_4$ (YLF) crystal under diode pumping has been intensively investigated. Recently a new laser host material for Nd has been proposed, $GdLiF_4$ (GLF). This crystal is iso-structural to YLF, presenting the same emission wavelengths. The spectroscopic properties of Nd in GLF are very similar to those of Nd:YLF, however GLF host allows higher concentrations of Nd^{3+} than in YLF. Nd:GLF laser also present low threshold and high efficiency of laser action under pulsed and CW pump [3,4].

On the other hand, high power – high brightness diode lasers are efficient sources to promote non-linear effects in laser media, for example up-conversion fluorescence. Using this effect, there are

* Corresponding author.

0925-3467/00/$ - see front matter
PII: S0925-3467(99)00111-1

a variety of systems where the infrared pump radiation can be converted into visible fluorescence [5,6]. Most of the processes rely either on excited-state absorption (ESA) or energy-transfer up-conversion (ETU). The pumping-related up-conversion processes in Nd:YLF were initially investigated by Fan and Byer [7] where they observed a blue fluorescence at 412 nm with CW pumping at 590 nm. Length and Macfarlane [8] observed a non-linear absorption process associated with a cross-relaxation process resulting in a violet CW up-conversion lasing of Nd:YLF under 603.6 nm laser pumping. A similar up-conversion fluorescence in Nd:LaF_3 was also seen as a result of a sequential pumping scheme with both 788 nm and 591 nm laser excitations or by a single excitation at 578 nm. In both cases a violet CW neodymium up-conversion laser was obtained [9]. Recently Chuang and Verdún [10] observed yellow and blue fluorescences induced by laser excitations in the range of 785–811 nm in Nd:YLF.

In this paper, we report the determination of the spectroscopic properties of Nd-doped YLF and GLF crystals excited with high-power diode laser at 797 nm. Anti-Stokes emissions from upper excited Nd levels, at 430, 530, 590 and 650 nm were observed, as a result of two- and three-step excitations of the Nd^{3+} ions. These up-conversion processes constitute an important source of pumping loss in Nd laser systems, at the laser threshold condition, which is not well characterized in the literature and it is an important factor concerning high power, high efficiency diode-pumped Nd lasers.

2. Experimental methods

The Nd-doped crystals were obtained from our crystal growth laboratory. The rare-earth fluorides were synthesized from ultra-pure oxides, using the process of high-temperature hydrofluorination in a fluoridric acid (HF) and argon atmosphere. The GLF and YLF materials were then purified using the technique of zone refining at the melting temperature and under a continuous flux of HF. The Nd was introduced into the crystals in the growing stage. The crystals were grown by Czochralski technique, using an argon gas atmosphere. The studied Nd concentrations were 0.6% mol% (8.50×10^{19} cm^{-3}) for the YLF crystal and 2% mol% (2.85×10^{20} cm^{-3}) for the GLF crystal.

The infrared pumping was performed with a GaAlAs laser diode, model SDL-2382-P1. This pumping system is a broad-area laser (1×500 μm^2), 4W CW, operating at 797 nm. The diode laser beam was collimated by a diffraction-limited, N.A. $= 0.5$. $f = 8$ mm objective, corrected by a $3\times$ anamorphic prism pair (both from *Melles Griot* and focused by a single $f = 10$ cm lens. Close to the focus, and for a longitudinal range of 2 mm, the beam had a rectangular profile, with transverse dimensions of approximately 60×300 μm^2. The pumping excitation was in the π orientation.

For the emission measurements, the crystal was pumped either by the diode laser beam or by a Xenon lamp. Both light beams, chopped at 40 Hz, were focused on the sample with a 10 cm focal length lens. The visible Nd emission was detected with an EMI 9558 photomultiplier and analyzed with a 0.25 m (Kratos) monochromator. The luminescence signal was processed using a PAR lock-in amplifier. The lifetimes of excited Nd^{3+} ions were measured using a pulsed laser excitation (10 ns) from a nitrogen laser-pumped dye laser tuned to 413 nm. The time-dependence signal was detected by a fast S-20 extended-type photomultiplier detector and analyzed using a signal-processing Box-Car averager (PAR 4402).

3. Anti-Stokes emissions

The motivation for this work was the observation of an intense yellow emission from the active-medium sample inside the laser resonator under diode pumping, at room temperature. To characterize this luminescence, we measured the Nd anti-Stokes emission spectrum under the diode laser excitation. In Fig. 1, is shown the scheme of the up-conversion processes. The anti-Stokes emission spectrum obtained is shown in Fig. 2, where one can see the groups of sharp emission lines of Nd^{3+} ions at 430 nm ($^2P_{1/2} \rightarrow {}^4I_{9/2}$), 530 nm ($^4G_{7/2} \rightarrow {}^4I_{9/2}$), 590 nm ($^4G_{7/2} \rightarrow {}^4I_{11/2}$) and 650 nm ($^4G_{7/2} \rightarrow {}^4I_{13/2}$). Under pumping with 797 nm,

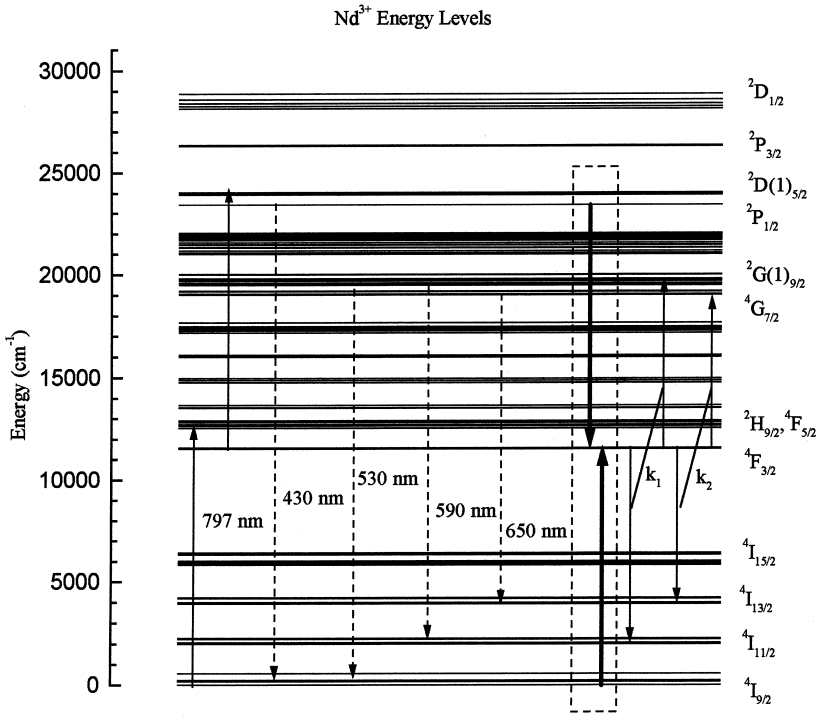

Fig. 1. Energy level diagram of Nd, showing the up-conversion processes under diode laser pumping at 797 nm and anti-Stokes emissions observed.

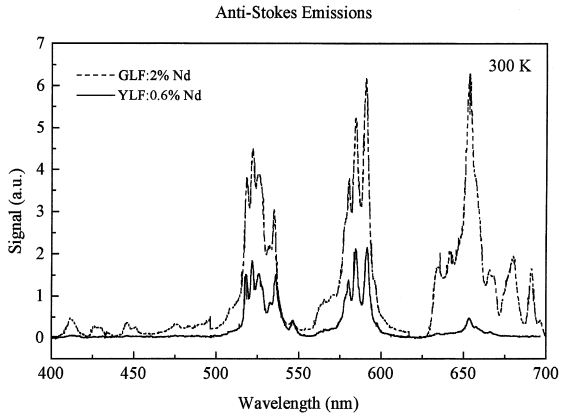

Fig. 2. Measured anti-Stokes emission observed with diode laser pumping at 300 K for YLF:0.6%Nd and GLF:2%Nd.

the Nd ions are prompt excited to $^2H_{9/2}$, $^4F_{5/2}$ manifold, from which they rapidly relax to the metastable $^4F_{3/2}$ level, that has a fluorescence lifetime of 538 μs for YLF [9] and 421 μs for GLF [11]. A second photon of 797 nm can excite few Nd ions from $^4F_{3/2}$ level to the $^2D(1)_{5/2}$ manifold, than relaxing mainly to the $^4G_{7/2}$ level. Another excitation can be induced by a 797 nm photon, which excites the $^2P_{3/2}$ level, being one of the possibilities due to the $^4F_{5/2} \rightarrow ^2P_{3/2}$ transition. These process are indicated as ESAPR. There are also the ETU-conversion processes involving two Nd^{3+} ions, leaving one ion in either the $^4G_{7/2}$ and manifolds or the $^2G(1)_{9/2}$ multiplet and the other ion in the states $^4I_{13/2}$ or $^4I_{11/2}$, respectively.

The more intense Nd anti-Stokes fluorescences are from the $^4G_{7/2}$ level. For these fluorescences, we determined the nonlinear intensity (I) dependence with the pumping beam power (P), as shown in Fig. 3, for the Nd:GLF. The data were fitted by an $I \propto P^n$ law, where n is the order of the process. All of the presented curves indicated a second-order processes.

The polarized emission spectra of the samples around the 1.05 μm region, at room temperature

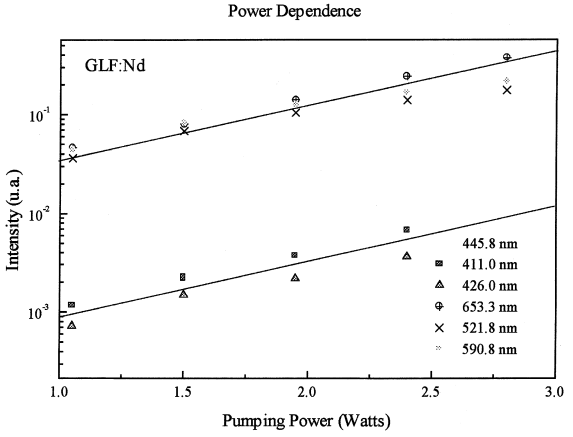

Fig. 3. Intensities of the anti-Stokes emissions at 300 K as a function of the pump power at 797 nm for Nd:GLF.

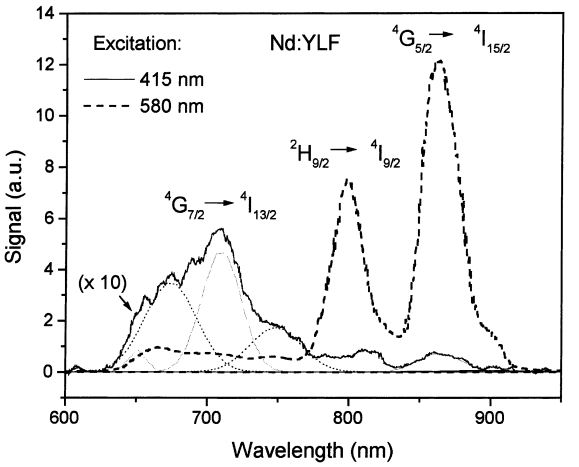

Fig. 4. The emission spectrum measured by exciting the Nd-doped YLF at 415 nm in the ($^4I_{9/2} \rightarrow {}^2D(1)_{5/2}$) transition and at 580 nm exciting the ($^4I_{9/2} \rightarrow {}^4I_{9/2}$) transition. Excitation at 415 nm makes the 805 nm emission to uppear. Gaussian decomposition is done to separate the undesirable emissions contributions to the $^2D(1)_{5/2} \rightarrow {}^4F_{3/2}$ transition.

were measured and the emission cross-section calculated. The ESA originates from the $^4F_{3/2}$ level, which is the upper laser level.

4. Excited state absorption

To evaluate the effect of the up-conversion in the laser efficiency of the Nd-doped laser crystals, we must know the fundamental spectroscopic parameters. The first parameter is the ESAPR cross-section (σ^*) related to the $^4F_{3/2} \rightarrow {}^2D(1)_{5/2}$ transition.

This parameter can be obtained from the $^2D(1)_{5/2} \rightarrow {}^4F_{3/2}$ emission spectrum near 805 nm, measured by exciting the $^4I_{9/2} \rightarrow {}^2D(1)_{5/2}$ transition at 415 nm using a monochromatic light from a 300 W xenon lamp (see straight line of Fig. 4). This excitation allowed us to separate this emission from the most intense ($^2H_{9/2} \rightarrow {}^4I_{9/2}$) transition emitting near 791 nm overlapping in the region of interest. When exciting the $^4G_{5/2}$ level with a monochromatic light at 580 nm, two intense emission peaks were observed at 791 and 860 nm due to the $^2H_{9/2} \rightarrow {}^4I_{9/2}$ and $^4G_{5/2} \rightarrow {}^4I_{15/2}$ transitions, as shown by dot line in Fig. 4. With the 415 nm excitation, the 805 nm-emission intensity of $^2D(1)_{5/2}$ level overtakes the 791 nm emission from the $^2H_{9/2}$ level, as shown by the Gaussian decomposition done in the emission spectra near the region of interest as shown in Fig. 5(a). This effect gives evidence of an existing cross-relaxation process between an excited Nd ion in $^2P_{1/2}$ state with a neighbor in the ground state $^4I_{9/2}$ (see a schematic representation shown in Fig. 1 for this process). This process short circuits the $^2H_{9/2}$ level and populates the $^4F_{3/2}$ level, besides quenching the $^2H_{9/2} \rightarrow {}^4I_{9/2}$ fluorescence. However, the remaining luminescence spectra still have some contributions at 791 and 825 nm due to the $^2H_{9/2} \rightarrow {}^4I_{9/2}$ and $^4G_{5/2} \rightarrow {}^4I_{15/2}$ transitions, as shown in Fig. 5(a) for both Nd:YLF and Nd:GLF crystals. The remaining spectrum between 795 and 815 nm is due to the $^2D(1)_{5/2} \rightarrow {}^4F_{3/2}$ transition. The same experimental procedure was used to obtain the emission spectra for both YLF and GLF crystals and afterwards to find the ESA line shape of interest and the absorption cross-section. The results are shown in Fig. 5(a).

We could obtain the ESAPR cross-section at 797 nm by comparing both emission intensities observed at 791 and 805 nm from different excitation wavelengths at 415 and 580 nm, respectively, working as a switch of one or another emission. This selective luminescence excitation technique was applied for estimating the absorp-

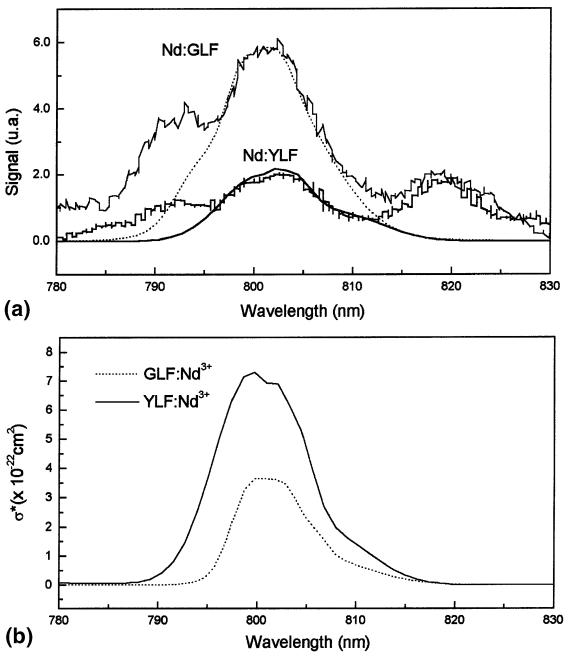

Fig. 5. (a) Details of emission line shape of the $^2D(1)_{5/2} \rightarrow {}^4F_{3/2}$ transition near 805 nm overlapping with the $^2H_{9/2} \rightarrow {}^4I_{9/2}$ emission at 795 nm obtained when exciting at 415 nm. (b) Excited state absorption of the transition $^2D(1)_{5/2} \rightarrow {}^4F_{3/2}$ transition.

tion cross-section of mentioned ESAPR process for both YLF and GLF crystals. The 805 nm-emission cross-section of $^2D(1)_{5/2}$ multiplet was estimated from the following relations

$$\sigma_e(^2H_{9/2} \rightarrow {}^4I_{9/2}) = (M_1)^{-1}\sigma_a(^4I_{9/2} \rightarrow {}^2H_{9/2}),$$

$$\sigma_e(^2D(1)_{5/2} \rightarrow {}^4F_{3/2}) \cong (R_1R_2)^{-1}(M_1)^{-1}\sigma_a(^4I_{9/2} \rightarrow {}^2H_{9/2}),$$

$$\sigma_e(^2D(1)_{5/2} \rightarrow {}^4F_{3/2}) = M_2\ \sigma_e(^2D(1)_{5/2} \rightarrow {}^4F_{3/2}),$$

R_1 is the ratio between the integrated 791 nm-emission from the $^2H_{9/2}$ level (excited at 580 nm) and the integrated 805 nm-emission from the $^2D(1)_{5/2}$ level obtained with the 415 nm excitation. R_2 is the factor that accounts for the absorption intensity differences verified when exciting these two distinct multiplets. M_i is the McCumber [12] factor at 300 K defined in Eq. (1). The absorption cross-section of $^4I_{9/2} \rightarrow {}^2H_{9/2}$ transition was calculated from the absorption spectra and has a value of 4.5×10^{-20} cm^2 at 797 nm for Nd:YLF. The ESAPR absorption cross-section of the $^2D(1)_{5/2} \rightarrow {}^4F_{3/2}$ transition estimated for both Nd:YLF and Nd:GLF crystals is shown in Fig. 5(b). The obtained values of $(R_1;\ R_2)$ are (450; 8) for YLF and (350; 6) for GLF crystals. By using these experimental parameters, it was possible to calculate the ESAPR absorption cross-sections (at 797 nm) of 6.4×10^{-22} cm^2 for Nd:YLF and 2.4×10^{-22} cm^2 for Nd:GLF. These small values of ESAPR cross-sections fairly agree with the theoretical value of 1.4×10^{-23} cm^2 obtained by Guyot et al. [13] for Nd:YLF, from the Judd–Ofelt theory [14,15].

The McCumber factor M_i was calculated using the following expression derived from McCumber relations [14] that connect the emission and absorption cross-sections

$$M_i = \left(\frac{N_2}{N_1}\right)_e \exp(-\hbar\omega/KT), \quad (1)$$

where $(N_2/N_1)_e$ is the ratio at thermal equilibrium of the two excited state populations involved in the transition. It is calculated by the Boltzman law and requires the energies of the Stark sub-levels.

5. Energy transfer up-conversion process

In this section, basic aspects of ETU [16] are discussed. The ETU process, in which an excited ion transfers non-radiactively its energy to an already excited neighboring ion, is one of the most efficient up-conversion mechanisms. ETU has been observed in a variety of systems, and in most of them it is the dominant process. The crystallographic structure of the system and the dopant concentration determine the spatial distribution as well as the nature of the ion pairs which are formed in the host lattice.

Fig. 6 shows schematically the relaxation process of an isolated pair of ions with equal energy spacing between the states 1, 2 and 3. After excitation of both ions to state 2 several relaxation processes can take place: one ion can be populated with a rate constant K (in this case $K = k_1 + k_2$, as shown in Fig. 1 by a non-radiative energy transfer

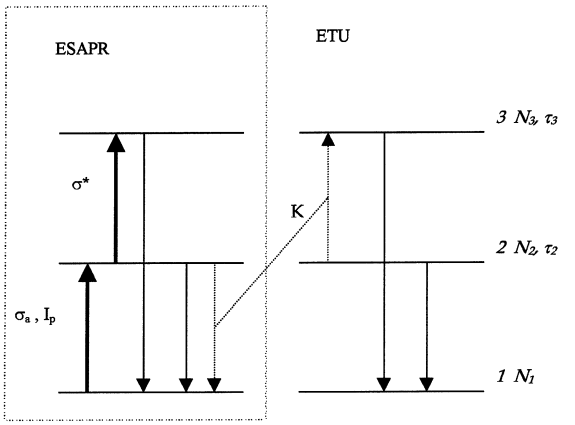

Fig. 6. Scheme of the energy levels and mechanisms involved in a simplified model of the optical cycle.

from its partner, this is the ETU process which leads to up-conversion luminescence from state 3. Once excited, both ions can individually relax from 2 to 1 with a lifetime τ_2. State 3 can in principle relax to both states 2 and 1. Populating state 2, in a subsequent relaxation from state 3, does not lead to a situation from which a further ETU process could take place and therefore does not influence population 3 any more. Thus only the total relaxation time from state 3 (and not its branching) is relevant for the temporal behavior of population N_3.

Assuming a dipole–dipole interaction between two Nd^{3+} ions in the excited state separated by the distance R, the microscopic ETU rate is given by $K_{D-A}(R) = (C_{D-A}/R^6)$, where C_{D-A} is the transference constant (cm^6/s) [17,18] for two ETU processes. The most important ETU processes are those indicated in the following for Nd:YLF crystals, as has been indicated by Pollnau et al. [19]

$$(k_1) \quad {}^4F_{3/2} \rightarrow {}^4F_{11/2} : {}^4F_{3/2} \rightarrow {}^2G(1)_{9/2},$$

$$(k_2) \quad {}^4F_{3/2} \rightarrow {}^4F_{11/2} : {}^4F_{3/2} \rightarrow {}^4G_{7/2}.$$

Considering a random ion distribution in the crystal, it is possible to define the function which express the fraction of finding Nd pairs as the closest neighbor inside of a shell between the distances R and $R + dR$. Since the $4f^N$ orbital of the (3+) rare-earth ions is always shielded by the most external fulfilled orbital ($5p^6$), one expects a negligible interaction between them in the ground state which, in turn, produces no tendency for either preference or rejection of a closer pair configurations away from statistical distribution. This argument justifies the use of a random distribution of Nd ions in the host at relatively high concentration ($x_2 > 0.005$), in the de-excitation model. This function was successfully applied to describe the cross-relaxation process between trivalent rare-earth ions in YLF crystal [20].

The ion distribution function, $f(R)$, is given by

$$f(R) = \frac{4\pi R^2}{AR_0^3} x_2 (1 - x_2)^{\frac{3}{4}\pi R^3/R_0^3 - 2}, \tag{2}$$

where $x_2 = N_2/N_{Y,Gd}$ is the mol fraction of excited Nd ions in the ${}^4F_{3/2}$ state (indexed by number 2 in the rate-equations scheme), and $R_0^3 = 1/N_{Y,Gd}$, ($R_0 = 4.16$ Å for the YLF and 4.21 Å for GLF). A is the normalization constant obtained from the relation: $A = \int_{R_{min}}^{\infty} f(R)dR$, where R_{min} is the nearest-neighbor (Y–Y or Gd–Gd) distances approximately equal to 3.72 Å.

The average value of the ETU probability k_i (s^{-1}) can be determined using the following expression

$$k_i = C_6 \left\{ \int_{R_{min}}^{\infty} \left[\left(\frac{1}{R^6} \right) f(R)\, dR \right] \right\}, \tag{3}$$

$C_6 = R_c^6/\tau_r$, where τ_r is the radiative lifetime of ${}^4F_{3/2}$ level. R_c is the critical distance for which excitation transfer and spontaneous emission of the sensitizer have equal probabilities. R_c can be written as

$$R_c^6 = \tau_r \left(\frac{1}{2\pi} \right)^4 \left(\frac{6c}{n^2} \right) \frac{g_l}{g_u} \int \sigma^*(\lambda)\sigma_e(\lambda)\, d\lambda, \tag{4}$$

where $\sigma^*(\lambda)$ represents the ESA cross-section spectrum of ${}^4F_{3/2} \rightarrow {}^2G(1)_{9/2}$ involved in k_1 and ${}^4F_{3/2} \rightarrow {}^4G_{7/2}$ in k_2 transitions ETU processes. $\sigma_e(\lambda)$ is the emission cross-section spectrum of ${}^4F_{3/2} \rightarrow {}^4F_{11/2}$ transition, n the refractive index and g_l and g_u are the lower and upper level degeneracies of donor. The ESA σ^* around 1.32 and 1.06 μm, was used from reference by Guyot et al. [21]. By substituting $f(R)$ in Eq. (4), one obtains k_1 and k_2 and subsequently $K_{ETU} = k_1 + k_2$. The result

shows that K_{ETU} is a linear function of the N_2 (the $^4F_{3/2}$ population of Nd ions) given by:

$$K_{ETU} = 2.66 \times 10^{-14}\ N_2\ (\mathrm{Nd:YLF}),$$
$$K_{ETU} = 2.60 \times 10^{-14}\ N_2\ (\mathrm{Nd:GLF}).$$

Taking $K_{ETU} = K$, it is then easily calculated from the N_2 population, given in cm^{-3}. Our results show that the $K(s^{-1})$ constant depends linearly on the Nd ($^4F_{3/2}$) population (N_2), which agrees with the up-conversion parameter found in the literature for YLF [15,19], for pumping intensity up to 0.1 KW/cm^2. As a consequence, the ETU probability rate increases with the laser pumping intensity and as well as the losses due to this process.

6. Determination of the anti-Stokes emission probabilities

The probability rate of an radiative transition between two distinct multiplets J and J' can be obtained from the well-known relation

$$A(J \to J') = \frac{64\pi^4 e^2}{3h(2J+1)\lambda^3}\frac{n(n^2+2)^2}{9} \times \sum_{t=2,4,6} \Omega_t \mid \langle SLJ \mid U^{(t)} \mid S''L'J' \rangle \mid^2, \tag{5}$$

where Ω_t are the Judd–Ofelt parameters which are dependent on the strength and symmetry of local field. Also, the radiative lifetime of an excited state (J) can be obtained by

$$\tau_R = \sum_J [A(J,J')]^{-1}. \tag{6}$$

Analysis of oscillator strengths of dipole-forced electronic transitions of 3+ rare-earth ions in solids are widely used by applying the Judd–Ofelt theory [12,13,22]. We used the same approach to calculate Ω_t in Nd:GLF as has been done for Nd:YLF crystal [23]. The calculated values of Ω_t for Nd:GLF are:

$$\Omega_2 = 0.905 \times 10^{-20}\ \mathrm{cm}^2,$$
$$\Omega_4 = 2.47 \times 10^{-20}\ \mathrm{cm}^2,$$
$$\Omega_6 = 4.92 \times 10^{-20}\ \mathrm{cm}^2.$$

Table 1
Relevant spectroscopic parameters for upper laser level population calculation, accounting for the up-conversion losses, in Nd:YLF and Nd:GLF

	YLF	GLF
[Nd](cm^{-3})	8.5×10^{19}	2.85×10^{20}
σ_a (cm^2)	3.2×10^{-20}	2.1×10^{-20}
σ^* (cm^2)	6.4×10^{-22} 1.4×10^{-23} [a]	2.4×10^{-22}
τ_2(μs)	538	421
τ_3(μs)($^4G_{7/2}$)	150	183
$\tau_{31}(s^{-1})$	3256	2974
$\tau_{32}(s^{-1})$	186 [b]	196
Nd–Nd interaction	$C_{D-A}(cm^6/s)$	R_c(Å)
($^4F_{3/2}/^4F_{11/2}$) – 1.05 μm	1.36×10^{-37}	20.4
($^4F_{3/2}/^4F_{13/2}$) – 1.3 μm	1.83×10^{-37}	21.4

[a] Ref. [16]. [b] Ref. [23].

By using the Ω_t values and the matrix elements $U^{(t)}$ for Nd^{3+} obtained from the literature [24], it was possible to calculate the radiative transition probabilities for all the up-conversion emissions which are relevant for the diode-pumped Nd-laser system. These emissions are those from the $^4G_{7/2}$ level, labeled as level 3 in the simplified laser system scheme (Fig. 6). Now we can compute the total radiative rate of the transitions ending below the metastable $^4F_{3/2}$ level, $(\tau_{31})^{-1}$, and the total of radiative transitions contributing for the $^4F_{3/2}$ population, $(\tau_{32})^{-1}$. The radiative transitions contributing for $(\tau_{31})^{-1}$ are those from $^4G_{7/2}$ to $^4I_{9/2}$, $^4I_{11/2}$, $^4I_{13/2}$ and $^4I_{15/2}$, respectively. The radiative transitions from $^4G_{7/2}$ to $^2H_{9/2}$ and $^4F_{3/2}$ are the ones contributing for $(\tau_{32})^{-1}$. The calculated radiative rates $(\tau_{31})^{-1}$, $(\tau_{32})^{-1}$ and the total (τ_3) lifetime of $^4G_{7/2}$ level for YLF and GLF crystals are shown in Table 1.

7. Rate equations and up-conversion losses evaluation

Let us consider a simplified system represented in Fig. 6. In this system there are three possible up-conversion processes: (1) ESAPR: ESA of pump radiation at 797 nm; (2) ETU: energy transfer up-conversion by cross-relaxation; and (3) ESALR: ESA of laser radiation at 1.05 μm, but in

the absence of laser action, ESALR can be disregarded. The ions are excited from the ground level $1(^4I_{9/2})$ to the upper level $2\,(^4F_{3/2})$ by the pumping radiation. A second pump photon or the ETU processes promote the system to level 3 (*the levels between* $^2P_{1/2}$ and $^4G_{7/2}$). The ions in level 3 can either directly decay to the ground state 1 or to the de-excited level 2. The populations of these levels are then given by:

$$\begin{aligned}
\frac{dn_1}{dt} &= -n_1\sigma_a I_p + \frac{n_2}{\tau_2} + \frac{n_3}{\tau_{31}} + K n_2^2,\\
\frac{dn_2}{dt} &= \sigma_a I_p n_1 - \frac{n_2}{\tau_2} - \sigma^* I_p n_2 - 2K n_2^2 + \frac{n_3}{\tau_{32}},\\
\frac{dn_3}{dt} &= n_2\sigma^* I_p - \frac{n_3}{\tau_3} + K n_2^2,\\
n_1 + n_2 + n_3 &= 1,
\end{aligned} \tag{7}$$

where, n_1, n_2 and n_3 are the normalized population of levels of 1, 2 and 3, respectively. The normalized population is given by $n_i = (N_i/N_0)$, where N_0 is the Nd concentration in the crystal (given in cm^{-3}). σ_a and σ^* are the cross-sections of the fundamental and the ESA of pumping radiation at 797 nm (ESAPR), respectively. I_p is the pumping intensity and τ_2 and τ_3 are the lifetimes of levels 2 ($^4F_{3/2}$) and 3 ($^4G_{7/2}$). The calculated values of all parameters are shown in Table 1.

At equilibrium, the system must obey the condition

$$\frac{dn_1}{dt} = \frac{dn_2}{dt} = \frac{dn_3}{dt} = 0. \tag{8}$$

The equilibrium population for the level 2 is then given by

$$n_2 = \frac{\sqrt{\varepsilon^2 + \delta\rho} - \varepsilon}{\delta},$$

where,

$$\begin{aligned}
\varepsilon &= (I_p\sigma^*\tau_2\tau_3) + \tau_{31} + I_p\sigma_a\tau_2\tau_{31} + I_p^2\sigma_a\sigma^*\tau_2\tau_3\tau_{31},\\
\delta &= 2K\tau_2(\tau_3 + \tau_{31} + I_p\sigma_a\tau_3\tau_{31}),\\
\rho &= 2I_p\sigma_a\tau_2\tau_{31}.
\end{aligned} \tag{9}$$

Expression (9) can be solved for I_p, thus leading to

$$I_{tu} = \frac{\alpha - \sqrt{\alpha^2 - \beta\gamma}}{\gamma},$$

where

$$\begin{aligned}
\alpha &= \tau_2\left[n_t\sigma^*\tau_3 + (n_t - 1 + Kn_t^2\tau_3)(\sigma_a\tau_{31})\right],\\
\beta &= 2n_t[Kn_t\tau_2(\tau_3 + \tau_{31}) + \tau_{31}],\\
\gamma &= 2n_t\sigma_a\sigma^*\tau_2\tau_3\tau_{31},
\end{aligned} \tag{10}$$

where n_2 was renamed as n_t, and I_p was renamed as I_{tu}, expliciting the emphasis on the laser threshold conditions, considering the up-conversion losses (I_{tu} mens the laser threshold intensity in the presence of up-conversion losses).

Considering now only the simplified rate equations model without including the excited state absorption (ESAPR) and the energy transfer up-conversion (ETU), the equilibrium population n_t of level 2 is given by the well known expression

$$n_t(\sigma^* = 0,\ K = 0) = \frac{I_p\sigma_a}{\sigma_a I_p + 1/\tau_2}. \tag{11}$$

On the other hand, expression (11) can be solved for the threshold condition where $I_p = I_t$ (where I_t is the laser threshold intensity without considering the up-conversion losses), leading to the following expression

$$I_t = I_s\frac{n_t}{1 - n_t}, \tag{12}$$

where $I_s = (\sigma_a\tau_2)^{-1}$ is the saturation intensity. A correction to this simplified model for the pumping process (Eq. (12)) can be implemented by defining a pumping efficiency given by

$$\eta_{(n_t)} = \frac{I_t(n_t)}{I_{tu}(n_t)} \tag{13}$$

such that the actual threshold pumping intensity can be obtained by using expression (12), when divided by η.

The theoretical values for the threshold pumping intensity, given by expression 12 corrected by the pumping efficiency η, as a function of the laser thresold population, are plotted in Fig. 7 (left scale) for the Nd:YLF and Nd:GLF crystals considered in this study. It can be seen that, due to the nonlinear up-conversion population losses, a threshold population above approximately

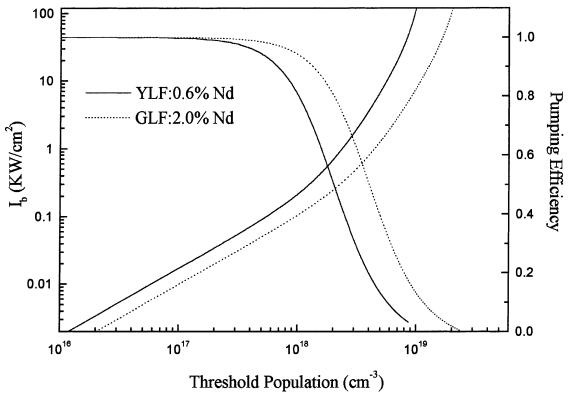

Fig. 7. Threshold pumping intensity (left-hand scale) and pumping efficiency (right-hand scale) as function of the laser threshold population, for the laser crystals considered in the study.

8.5×10^{18} cm^{-3} for YLF, and 2.1×10^{19} cm^{-3} for GLF cannot be obtained by increasing the pumping intensity. In this same figure, the pumping efficiency as defined by (13) is plotted as a function of the threshold population (right scale). It is important to mention that the pumping intensity range covered by Fig. 7, corresponds to real possibilities of Nd-pumping intensities because it is always below the crystal breakdown intensity which is found be in the order of 20 KW/cm^2 for Nd:YLF [25].

8. Discussion

It is seen that (Fig. 7) the up-conversion processes impose dramatical limitations in the maximum achievable inverted population for the two systems. In both cases, the maximum inverted population is of the order of one-tenth of the total population. Therefore, higher Nd concentrations allow for higher gain coefficients, which favors the GLF crystal as a laser host, where concentration of 5 mol% can be achieved [11]. In these cases, the maximum gain is 2.6 cm^{-1} (1 mol%) for Nd:YLF and 6.7 cm^{-1} (5 mol%) for Nd:GLF, corresponding to the maximum population inversion of one-tenth of the total population available in both systems. It must be stressed that the pumping efficiencies for these systems, in this limit, are almost zero (see Fig. 7). On trying to work on keeping the 100% pumping efficiency, maximum gain, the inverted populations are only 5×10^{17} cm^{-3} and 1×10^{17} cm^{-3} for Nd:GLF and Nd:YLF, that corresponds, respectively to small gain coefficients of 0.05 and 0.02 cm^{-1}. In both cases, these small gain coefficients are too small for practical systems where internal laser losses are inevitable and significant output mirror transmissions are often desirable. Long media (several cm long) can compensate these small gain coefficients, but in this case the great advantage of dipole pumped systems, compactness, is lost. For the majority of the Nd laser systems, a trade-off between pumping efficiencies and overall laser efficiency must be achieved.

9. Conclusions

We have studied the pumping-related up-conversion processes in Nd laser crystals. They are significant under typical diode laser pumping intensities and these processes depend non-linearly on the pumping power. The peak of the ESA cross-section for the pumping radiation at 797 nm was evaluated as 6.4×10^{-22} cm^2 (YLF) and 2.4×10^{-22} cm^2 (GLF) at 797 nm. A model to estimate the probability of the ETU process based on the Förster–Dexter method was proposed and the ETU parameters were calculated. By solving the rate equations for the system under continuous pumping, it was possible to estimate the up-conversion efficiency near threshold conditions for the two Nd systems. By using the ESAPR absorption cross-section, at 797 nm, obtained for Nd:YLF in [14] in the rate equations solution, we got the same results expressed by Fig. 7. That means that the ESAPR process does not have important effect on the up-conversion losses in Nd laser system because this process involves a very small excited absorption cross-section. Only the ETU processes (k_1 and k_2) are responsible for the non-linear losses present in the system with the threshold population increasing beyond 5×10^{17} cm^{-3}. These processes cause important losses for the Nd laser system, increasing the power intensity to reach the laser threshold conditions.

The threshold pumping efficiency, as defined in this work, has great importance, for instance, for regenerative amplifiers and Q-switched lasers, that have a low Q period in part of their operation cycle. In both cases, the system must achieve the highest possible gain (inverted population), while compactness is also desired. This is specially important for Q-switched systems, where the pulse duration is a minimum for minimum cavity length and maximum initial gain ($2N_t\sigma_s l$). But, in order to achieve high-optical efficiencies, one must minimize the non-linear losses, so the gain coefficient must be kept moderate. Therefore, the present analysis can be very helpful when designing an optimized Q-switched Nd laser, allowing the determination of the best trade-off between pumping intensity and active medium length for maximum peak power and/or pulse energy. Once determined this optimum pumping intensity, the system is still scalable in energy by increasing the transverse active area. In the case of regenerative amplifiers even side pumping can be an advantageous alternative, because besides keeping the gain moderate (and therefore the optical efficiency high), it presents less thermal problems.

Finally, we must highlight the Nd:GLF as a promising laser medium for amplifier or Q-switched systems.

Acknowledgements

This work was supported by FAPESP under grant 93/4999-7 and PADCT-FINEP under contract number 54910293000. Two authors (Courrol and Maldonado) were supported by post-doctoral scholarships from FAPESP.

References

[1] R. Scheps, Appl. Opt. 1 (28) (1989) 89.
[2] N.P. Barnes, M.E. Storm, P.L. Cross, M.W. Skolaut, IEEE J. Quant. Electron. 26 (3) (1990) 558.
[3] X.X. Zhang, M. Bass, A.B. Villaverde, J. Lefaucher, A. Pham, B.H.T. Chai, Appl. Phys. Lett. 62 (11) (1993) 1197.
[4] E.P. Maldonado, I.M. Ranieri, S.P. Morato, N.D. Vieira Jr., Adv. Solid State Lasers 10 (1997) 444.
[5] C.Y. Chen, W.A. Sibley, D.C. Yeth, C.A. Hunt, J. Lumines. 43 (1989) 185.
[6] R.M. Macfarlane, F. Tong, A.J. Silversmith, W. Lenth, Appl. Phys. Lett. 52 (16) (1988) 1300.
[7] T.Y. Fan, R.L. Byer, J. Opt. Soc. Am. B 3 (11) (1986) 1519.
[8] W. Lenth, R.M. Macfarlane, Lasers, Opt. and Photon. News, 1992.
[9] W. Lenth, R.M. Macfarlane, J. Lumines. 45 (1–6) (1990) 346.
[10] T. Chuang, H.R. Verdún, IEEE J. Quant. Electron. 32 (1) (1996) 79.
[11] X.X. Zhang, A.B. Villaverde, M. Bass, B.H.T. Chai, H. Weidner, R.I. Ramotar, R.E. Peale, J. Appl. Phys. 74 (2) (1993) 790.
[12] D.E. McCumber, Phys. Rev. 136 (4) (1964) 954.
[13] Y. Guyot, H. Manaa, J.Y. Rivoire, R. Moncorgé, N. Garnier, E. Descroix, M. Bom, P. Laporte, Phys. Rev. B 51 (2) (1995) 784.
[14] J. Judd, Phys. Rev. 127 (3) (1962) 750.
[15] G.S. Ofelt, J. Chem. 37 (750) (1962).
[16] F. Auzel, J. Lumines. 45 (1–6) (1990) 341.
[17] T. Förster, Z. Naturforsch 49 (1949) 321.
[18] D.L. Dexter, J. Chem. Phys. 21 (5) (1952) 836.
[19] M. Pollnau, P.J. Hardman, W.A. Clarkson, D.C. Hanna, Opt. Commun. 147 (1–3) (1998) 203.
[20] L. Gomes, L.C. Courrol, L.V.G. Tarelho, I.M. Ranieri, Phys. Rev. B 54 (6) (1996) 3825.
[21] Y. Guyot, R. Moncorge, J. Appl. Phys. 73 (12) (1993) 8526.
[22] C.Y. Chen, W.A. Sibley, D.C. Yeh, C.A. Hunt, J. Lumines. 43 (1989) 185.
[23] C. Li, Y. Guyot, C. Linares, R. Moncorgé, M.F. Joubert, OSA Proc. Adv. Solid-State Laser 5 (1993) 9195.
[24] W.T. Carnall, H. Crosswhite, H.M. Crosswhite, unpublished.
[25] M. Lopes Filho, Master Dissertation, IPEN/CNEN-SP, 1999.